

## Soft perpendicular magnetization and spin reorientation transition of Fe films on NiAl(001)

Yin-Chih Lin<sup>1†</sup>, Chii-Bin Wu<sup>1,2†</sup>, Wei-Shu Li<sup>1</sup>, Ying-Chin Chen<sup>1</sup>, Zheng-Yuan Huang<sup>1</sup>, Wen-Chin Lin<sup>3\*</sup>, and Minn-Tsong Lin<sup>1,4\*</sup><sup>1</sup>Department of Physics, National Taiwan University, Taipei 106, Taiwan<sup>2</sup>Department of Physics, Chung Yuan Christian University, Chungli 320, Taiwan<sup>3</sup>Department of Physics, National Taiwan Normal University, Taipei 116, Taiwan<sup>4</sup>Institute of Atomic and Molecular Sciences, Academia Sinica, Taipei 106, Taiwan

E-mail: wclin@ntnu.edu.tw; mtlin@phys.ntu.edu.tw

Received November 21, 2013; accepted December 24, 2013; published online January 21, 2014

Ultrathin Fe films were deposited on NiAl(001) for studies of their magnetic properties and crystalline structures. Thickness-driven perpendicular to in-plane spin reorientation transition was observed at a thickness of  $\sim 4$  monolayers (MLs) at room temperature without structural variation. At less than the critical thickness, the Fe film's easy axis is perpendicular to the surface plane with a small coercive field ( $H_c \approx 1$  Oe), which was much smaller than that of other systems with perpendicular anisotropy. The Fe/NiAl(001) system revealed an extremely soft perpendicular magnetization. At more than the critical thickness, the easy axis lays in the surface plane. The magnetic anisotropy terms were calculated and discussed through a phenomenological model. The weaker surface anisotropy might be attributed to the reconstructed NiAl(001) surface.

© 2014 The Japan Society of Applied Physics

Iron is a critical and interesting element in fundamental research of magnetism because it is located between antiferromagnetic Mn and ferromagnetic Co on the Bethe–Slater curve. It has a high magnetic moment of  $2.18 \mu_B/\text{atom}$ <sup>1)</sup> compared to Co ( $\sim 1.6 \mu_B/\text{atom}$ )<sup>2)</sup> and Ni ( $\sim 0.57 \mu_B/\text{atom}$ )<sup>2)</sup>. Iron exhibits different crystalline structures, e.g., bcc, fcc and hcp structures. Experimental results show that epitaxial growth between an ultrathin film and a substrate could create and control different metastable structures, e.g., bcc-Fe/Ag(001),<sup>3,4)</sup> bcc-Fe/Au(001),<sup>5)</sup> fcc–bcc Fe/Cu<sub>3</sub>Au(001),<sup>6)</sup> and fcc–bcc Fe/Cu(001).<sup>7,8)</sup> In those cases, ultrathin Fe films were deposited on fcc substrates at a rotation of  $45^\circ$  in the  $ab$  plane to match the epitaxial condition. These systems exhibit a thickness-driven perpendicular to in-plane spin reorientation transition (SRT). In Fe/Cu<sub>3</sub>Au(001) and Fe/Cu(001) systems, the SRT transition region is almost the same as the fcc to bcc(011) crystalline transition.<sup>6–8)</sup> Thus the SRT in those systems is likely the result of structural transformation. In the Fe/Ag(001) case, the SRT transition region appears at 6–7 monolayers (ML) at room temperature with a stable bcc(001) structure. In this case, SRT is caused by the competition between the surface anisotropy and the shape anisotropy. For the surface anisotropy, the interfacial condition between the thin film and the substrate also plays an important role. The interfacial conditions, e.g., surface reconstruction<sup>9)</sup> and roughness,<sup>10)</sup> are crucial considerations for SRT studies.

The lattice constant of bcc-Fe is  $2.87 \text{ \AA}$ , as shown in Fig. 1(a). The bcc-NiAl(001) substrate with a lattice constant of  $2.89 \text{ \AA}$  is also suitable for epitaxial growth. Ultrathin Fe films on NiAl(001) are weakly strained because of low lattice mismatch between bcc-Fe and NiAl(001) of around 1%, as shown in Fig. 1(b). Moreover, the NiAl(001) surface reveals a special reconstructed surface of  $c(\sqrt{2} \times 3\sqrt{2})R45^\circ$  after annealing treatment exceeding 800 K. The top layer of NiAl(001) is determined by the annealing temperature, e.g., Al termination at an annealing temperature of 800 to 1400 K and Ni termination at an annealing temperature exceeding 1400 K.<sup>11,12)</sup>

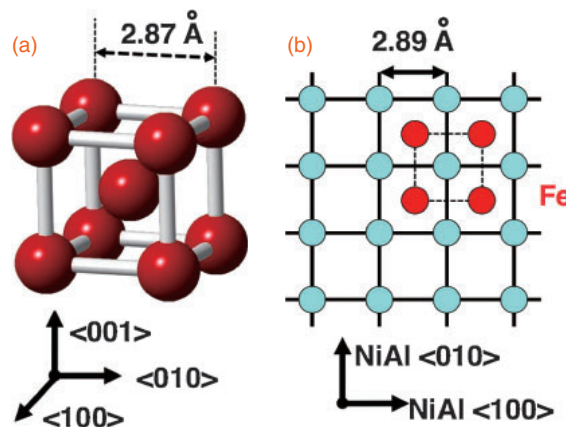
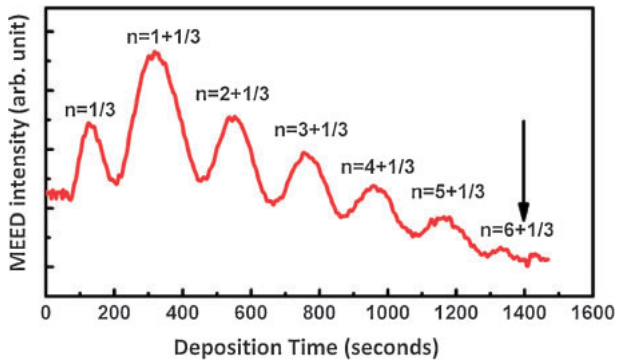


Fig. 1. (a) Crystalline structure of bcc-Fe ( $a = b = c = 2.87 \text{ \AA}$ ).

(b) Illustrations of epitaxially grown Fe on bcc-NiAl(001). The ocean blue circles indicate atoms on the top surface of unreconstructed NiAl(001). The red circles represent the cubic cells of bcc-Fe.

The experiment was performed in situ in a UHV system with a base pressure of  $5 \times 10^{-10}$  mbar. The NiAl(001) single-crystal substrate was cleaned by cycles of Ar<sup>+</sup> sputtering with a kinetic energy of 2 keV and subsequently annealed at 1000 K for 1 h. After the substrate was cooled to room temperature, a clean NiAl(001) surface was obtained, as verified by low-energy electron diffraction (LEED) and Auger electron spectroscopy (AES). The ultrathin Fe film was deposited on the clean NiAl(001) at room temperature by electron-beam-heated thermal evaporation at a deposition rate of 180–220 s/ML. During the evaporation process, the growth mode was monitored in real time by medium energy electron diffraction (MEED). The deposition rate with an accuracy of 0.1 ML was calibrated by the period of MEED oscillation.<sup>13)</sup> The crystalline structure was calculated by LEED measurement. LEED patterns provide the surface structure and the in-plane lattice constant, whereas information on the interlayer distance is obtained from the LEED- $I(E)$  result.<sup>14,15)</sup> The magnetic properties were investigated in situ by AC magneto-optical Kerr effect (MOKE) measurements in both polar and longitudinal geometries. To measure the ultrasmall signals and increase signal sensitivity, photoelastic

<sup>†</sup>These authors contributed equally to this work.



**Fig. 2.** MEED intensity oscillations of Fe deposited on NiAl(001) at room temperature, measured with an electron beam energy of 3.5 keV at a glancing angle of 5°. (The arrow indicates a closed shutter.)

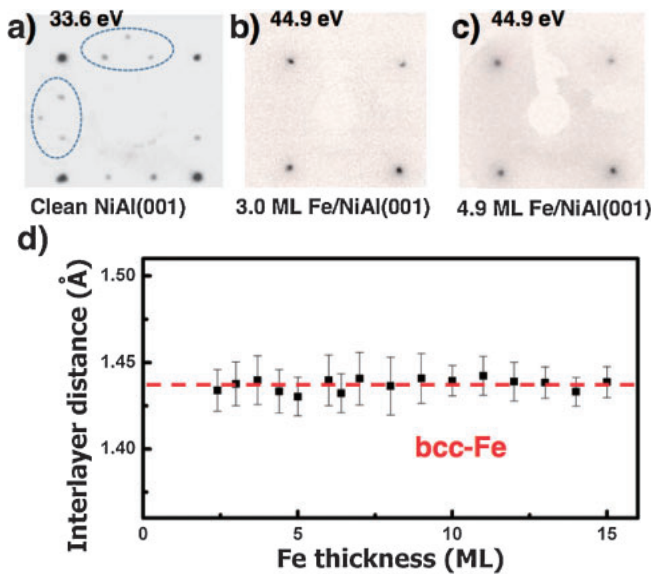


**Fig. 3.** (a) LEED pattern of clean NiAl(001), where the dotted marks indicate a  $c(\sqrt{2} \times 3\sqrt{2})R45^\circ$  superstructure. (b, c) LEED patterns of 3.0 and 4.9 ML Fe deposited on NiAl(001). (d) Interlayer distance of 2.4–15.0 ML Fe on NiAl(001), as deduced from the LEED- $I(E)$  curves.

modulation and a lock-in amplifier were utilized on MOKE to investigate the hysteresis loops of the ultrathin films.

The thickness calibration and growth mode were measured using MEED oscillations. Figure 2 shows that the growth mode of Fe on NiAl(001) proceeds via a layer-by-layer model up to 7 ML. MEED intensity reached the first maximum peak after 1/3 of the layer-by-layer oscillation period. This might be because of the vacancy sites on the surface of NiAl(001). After sputtering and annealing, the LEED patterns revealed not only the  $p(1 \times 1)$  spots but also the  $c(\sqrt{2} \times 3\sqrt{2})R45^\circ$  superstructure on a clean NiAl(001) surface, as shown in Fig. 3(a). Such a reconstructed surface is not fully covered by aluminum and still has 1/3 vacancy sites on the top layer. After Fe was deposited on NiAl(001), it still revealed only  $p(1 \times 1)$  spots, as seen in Figs. 3(b) and 3(c). No obvious difference appears as the Fe thickness increases. This result also indicates that the in-plane lattice constant of Fe films is almost the same as that of NiAl(001) substrate (2.89 Å). The interlayer distance of ultrathin films was obtained by calculating the kinetic approximation of LEED- $I(E)$ .<sup>14,15</sup> The interlayer distance maintains almost the same

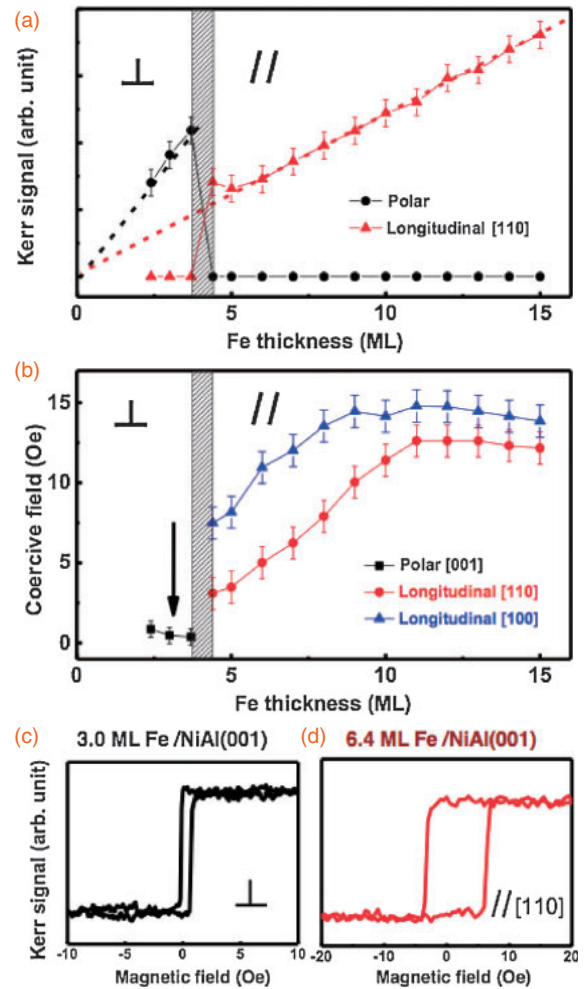


**Fig. 4.** (a) Saturated Kerr signal in polar (circle) and longitudinal (triangular) geometries as a function of Fe coverage measured at room temperature. Dashed lines are linear fits to the experimental data. (b) The coercive field in polar (circle) and longitudinal (triangular and square) geometries. (c) Hysteresis loop of 3.0 ML Fe on NiAl(001) in polar geometry. (d) Hysteresis loop of 6.4 ML Fe on NiAl(001) in longitudinal geometry.

value (1.43–1.44 Å in the Fe thickness range of 2.4–15 ML). These results imply that the crystalline structure of an ultrathin Fe film on NiAl(001) is close to bcc without significant expansion or compression.

The saturated magnetic signal of the films in the polar and the longitudinal (along the [110] direction) MOKE measurement is plotted as a function of the thickness in Fig. 4(a). The perpendicular to in-plane SRT appears at a thickness of  $\sim 4.0$  ML in Fig. 4(a). A comparison of the MOKE measurement along the [100] and [110] directions indicates that the coercive field measured along the [110] direction is smaller than that along the [100] direction. Therefore, we suppose that the easy axis in the thickness range of 4.4–15.0 ML is along the [110] direction of the Fe thin film, as shown in Fig. 4(b). This orientation might be due to an additional anisotropy resulting from the special superstructure of  $c(\sqrt{2} \times 3\sqrt{2})R45^\circ$  on the NiAl(001) surface. The hysteresis loop of 3.0 ML Fe on NiAl(001) is square in the polar MOKE geometry. The coercive field is approximately 1 Oe and apparently smaller than the case of 6.4 ML Fe on NiAl(001) in the longitudinal geometry, as Figs. 4(c) and 4(d) show. These results imply that the perpendicular Fe exhibits a soft

magnetic behavior. Furthermore, to investigate the temperature effect on the SRT behavior, we performed MOKE measurements at 110 K, according to which the SRT transition region was found not to vary significantly from the results at room temperature.

The easy axis of a magnetic thin film is determined by the effective magnetic anisotropy.<sup>16)</sup> The magnetic anisotropy usually consists of a series of terms of different physical origin. Examples include magneto-crystalline anisotropy, shape anisotropy, magneto-elastic anisotropy, and surface anisotropy. To assay this system, we use a phenomenological model<sup>16)</sup> to describe the thickness-driven SRT behavior. In this model the effective anisotropy  $K_{\text{eff}}$  is given by

$$K_{\text{eff}} = \frac{2K_s}{t} + K_v = \frac{2K_s}{t} + (K_{\text{me}} + K_{\text{shape}} + K_{\text{crystal}}), \quad (1)$$

where  $K_s$  is the surface anisotropy, which combines contributions from the thin film/substrate interface and the vacuum/thin film interface, and  $K_v$  is the volume contribution of anisotropy, which includes  $K_{\text{me}}$ ,  $K_{\text{shape}}$ , and  $K_{\text{crystal}}$ .  $K_{\text{me}}$  is the magneto-elastic anisotropy, which is related to the strain in the crystalline structure of thin films. The strain originates from the mismatch between the ultrathin film and the substrate.  $K_{\text{crystal}}$  is the magneto-crystalline anisotropy, which is related to the spin-orbit coupling in various crystalline structures.  $K_{\text{shape}}$  is the shape anisotropy, which is related to the demagnetization field induced by the geometrical shape of the sample. To clarify the reason for the SRT, we assayed several kinds of magnetic anisotropy in order. First, according to the LEED and LEED- $I(E)$  results, the crystalline structure of Fe/NiAl(001) maintains a bcc structure from a thickness between 2.4 and 15.0 ML. The  $c/a$  ratio of bcc-Fe is in a small variation region and very close to 1. Therefore, the SRT is not induced by the structural transition or the strain in the crystalline structure. According to previous studies, the bulk magneto-crystalline anisotropy of bcc-Fe is small and approximately  $3.62 \mu\text{eV}/\text{atom} = 4.8 \times 10^{-2} \text{MJ}/\text{m}^3$ .<sup>17)</sup> The magneto-elastic anisotropy and the bulk magneto-crystalline anisotropy are very small compared with the shape anisotropy and can be neglected. Consequently, the shape anisotropy and the surface anisotropy are the principal factors causing magnetic anisotropy and, as evaluated, the competition between them controls the easy axis in this system. The shape anisotropy of bcc-Fe is  $-132 \mu\text{eV}/\text{atom}$  from  $M_{\text{Fe}} = 2.18 \mu_{\text{B}}/\text{atom}$ <sup>1)</sup> and  $K_{\text{shape}} = -2\pi M^2$ . The SRT appears in the transition region at which the effective anisotropy starts to change sign from positive to negative. Accordingly, the following formula can be obtained:

$$K_s = -\frac{t_c}{2} \times K_v \simeq -\frac{t_c}{2} \times K_{\text{shape}}. \quad (2)$$

Based on Eq. (2), the surface anisotropy in the Fe/NiAl(001) system is deduced to be  $267.3 \mu\text{eV}/\text{atom}$ . For the purpose of comparison, the surface anisotropies, derived from the critical thickness according to Eq. (2), of Fe/Ag(001) and Fe/Au(001) are listed in Table I, together with a theoretical value of free-standing Fe film. It is clear that the Fe/NiAl(001) system has a smaller surface anisotropy than the Fe/Ag(001) system. Because the surface anisotropy is related to the interface between the thin film and the substrate, a possible

**Table I.** The SRT transition region, the coercive perpendicular field, and the surface magnetic anisotropy of similar ultrathin Fe films. The surface anisotropy of free-standing bcc-Fe is the result from theoretical calculation, and that of other systems are deduced from the critical thickness according to Eq. (2).

System	SRT region (ML)	$H_c$ (Oe)	$K_s$ ( $\mu\text{eV}/\text{atom}$ )
Free-standing bcc Fe			594.4 <sup>18,19)</sup>
bcc-Fe/Ag(001)	6.0–7.0 <sup>3)</sup>	60–80 ( $\perp$ ) <sup>3)</sup>	429.0 $\pm$ 33.0
bcc-Fe/Au(001)	2.0–2.3 <sup>5)</sup>	5–10 ( $\perp$ ) <sup>5)</sup>	141.9 $\pm$ 9.9
bcc-Fe/NiAl(001)	3.7–4.4	1 $\pm$ 0.5 ( $\perp$ )	267.3 $\pm$ 23.1

explanation for this result is surface reconstruction of NiAl(001). The NiAl(001) surface is not fully covered by Al and still has 1/3 vacancy sites. This partial covering might reduce the strength of the surface anisotropy. Thus, the SRT transition region is apparently reduced compared with that of the Fe/Ag(001) system.

In addition to the SRT phenomenon, the system exhibits soft perpendicular magnetization. In the thickness range of 2.4–3.7 ML, the coercive field of bcc-Fe with a perpendicular easy axis is very small ( $H_c \approx 1$  Oe), as already shown in Fig. 4(d). Such soft magnetic behavior is similar to that of Permalloy (NiFe), but the latter is observed only in the in-plane magnetization. The AES characterization shows no significant NiFe alloy formation at the interface. According to LEED- $I(E)$  measurement, the interlayer distance of 2.7 ML Fe is approximately  $1.44 \text{ \AA}$ , which is far below the interlayer distance of NiFe ( $1.77 \text{ \AA}$ ),<sup>20)</sup> indicating that Fe–Ni alloy formation at the Fe/NiAl interface is negligible. Consequently, both LEED- $I(E)$  and AES measurements can exclude the possibility of Fe–Ni alloy formation. Therefore, such soft perpendicular magnetization is most likely due to the intrinsic properties of the Fe ultrathin films on the NiAl(001) surface.

In summary, ultrathin bcc-Fe on NiAl(001) exhibits soft perpendicular magnetic behavior in the low thickness range. The coercive field is approximately 1 Oe and obviously smaller than that of other similar systems, e.g., Fe/Ag(001) and Fe/Au(001). Furthermore, the SRT critical thickness in this system is around 4 ML. In the transition region, the ultrathin film sustains a bcc structure with low strain. According to our calculation based on a phenomenological model, the surface anisotropy of the Fe/NiAl(001) system is  $267.3 \mu\text{eV}/\text{atom}$ . We suppose that such a small surface anisotropy in the Fe/NiAl(001) system could be attributed to the  $c(\sqrt{2} \times 3\sqrt{2})R45^\circ$  superstructure of NiAl(001).

**Acknowledgment** We would like to thank Sheng-Syun Wong for technical support. This study was supported in part by the National Science Council of Taiwan through Grant Nos. NSC 98-2120-M-002-010 and NSC 102-2120-M-002-005.

- 1) R. J. Hicken, S. J. Gray, A. Ercole, C. Daboo, D. J. Freeland, E. Gu, E. Ahmad, and J. A. C. Bland, *Phys. Rev. B* **55**, 5898 (1997).
- 2) R. F. Willis, J. A. C. Bland, and W. Schwarzacher, *J. Appl. Phys.* **63**, 4051 (1988).
- 3) Z. Q. Qiu, J. Pearson, and S. D. Bader, *Phys. Rev. Lett.* **70**, 1006 (1993).
- 4) R. K. Kawakami, E. J. Escorcia-Aparicio, and Z. Q. Qiu, *Phys. Rev. Lett.* **77**, 2570 (1996).
- 5) D. Wilgocka-Ślęzak, K. Freindl, A. Kozioł, K. Matlak, M. Rams, N. Spiridis, M. Ślęzak, T. Ślęzak, M. Zajęc, and J. Korecki, *Phys. Rev. B* **81**, 064421 (2010).

- 6) M.-T. Lin, J. Shen, W. Kuch, H. Jenniches, M. Klaua, C. M. Schneider, and J. Kirschner, *Phys. Rev. B* **55**, 5886 (1997).
- 7) J. Thomassen, F. May, B. Feldmann, M. Wuttig, and H. Ibach, *Phys. Rev. Lett.* **69**, 3831 (1992).
- 8) D. Li, M. Freitag, J. Pearson, Z. Q. Qiu, and S. D. Bader, *Phys. Rev. Lett.* **72**, 3112 (1994).
- 9) J. Lindner, P. Pouloupoulos, R. Nünthel, E. Kosubek, H. Wende, and K. Baberschke, *Surf. Sci.* **523**, L65 (2003).
- 10) P. Pouloupoulos, J. Lindner, M. Farle, and K. Baberschke, *Surf. Sci.* **437**, 277 (1999).
- 11) D. R. Mullins and S. H. Overbury, *Surf. Sci.* **199**, 141 (1988).
- 12) R.-P. Blum, D. Ahlbehrendt, and H. Niehus, *Surf. Sci.* **366**, 107 (1996).
- 13) M.-T. Lin, W. C. Lin, C. C. Kuo, and C. L. Chiu, *Phys. Rev. B* **62**, 14268 (2000).
- 14) W. C. Lin, B. Y. Wang, Y. W. Liao, K.-J. Song, and M.-T. Lin, *Phys. Rev. B* **71**, 184413 (2005).
- 15) M.-T. Lin, W. C. Lin, C. C. Kuo, and C. L. Chiu, *Phys. Rev. B* **62**, 14268 (2000).
- 16) L. Neel, *Compt. Rend.* **237**, 1468 (1953).
- 17) B. D. Cullity and C. D. Graham, *Introduction to Magnetic Materials* (Wiley-IEEE Press, New York, 2005).
- 18) J. G. Gay and R. Richter, *Phys. Rev. Lett.* **56**, 2728 (1986).
- 19) B. Y. Wang, N. Y. Jih, W. C. Lin, C. H. Chuang, P. J. Hsu, C. W. Peng, Y. C. Yeh, Y. L. Chan, D. H. Wei, W. C. Chiang, and M.-T. Lin, *Phys. Rev. B* **83**, 104417 (2011).
- 20) F. Michelini, L. Ressler, J. Degauque, P. Baulès, A. R. Fert, J. P. Peyrard, and J. F. Bobo, *J. Appl. Phys.* **92**, 7337 (2002).